In-situ TEM irradiation creep experiment revealing radiation induced dislocation glide in pure copper

Nargisse Khiara, Fabien Onimus, Stéphanie Jublot-Leclerc, Thomas Jourdan, Thomas Pardoen, Jean-Pierre Raskin, Yves Bréchet

▶ **To cite this version:**

Nargisse Khiara, Fabien Onimus, Stéphanie Jublot-Leclerc, Thomas Jourdan, Thomas Pardoen, et al.. In-situ TEM irradiation creep experiment revealing radiation induced dislocation glide in pure copper. Acta Materialia, 2021, 216, pp.117096. 10.1016/j.actamat.2021.117096 . in2p3-03324958

HAL Id: in2p3-03324958
https://in2p3.hal.science/in2p3-03324958v1

Submitted on 24 Aug 2021

HAL is a multi-disciplinary open access archive for the deposit and dissemination of scientific research documents, whether they are published or not. The documents may come from teaching and research institutions in France or abroad, or from public or private research centers.

L'archive ouverte pluridisciplinaire **HAL**, est destinée au dépôt et à la diffusion de documents scientifiques de niveau recherche, publiés ou non, émanant des établissements d'enseignement et de recherche français ou étrangers, des laboratoires publics ou privés.

Acta Materialia **216** (2021) 117096 https://doi.org/10.1016/j.actamat.2021.117096

In-situ irradiation creep experiment in a TEM revealing fast dislocation glide induced by irradiation in pure copper

Authors: Nargisse Khiara[(1)], Fabien Onimus[(1)], Stéphanie Jublot-Leclerc[(2)], Thomas Jourdan[(3)], Thomas Pardoen[(4)], Jean-Pierre Raskin[(5)], Yves Bréchet[(6)]

[(1)] Université Paris-Saclay, CEA, Service de Recherches Métallurgiques Appliquées, 91191, Gif-sur-Yvette, France
[(2)] Université Paris-Saclay, CNRS/IN2P3, IJCLab, 91405 Orsay, France
[(3)] Université Paris-Saclay, CEA, Service de Recherches de Métallurgie Physique, 91191, Gif-sur-Yvette, France
[(4)] Institute of Mechanics, Materials and Civil Engineering, UCLouvain, Place Sainte Barbe 2 L5.02.02, 1348, Louvain-la-Neuve, Belgium
[(5)] Institute of Information and Communication Technologies, Electronics and Applied Mathematics, UCLouvain, Place du Levant 2 L5.04.04, 1348, Louvain-la-Neuve, Belgium
[(6)] Science et Ingénierie des Matériaux et Procédés (SIMAP), Université Grenoble Alpes, 1130 rue de la Piscine BP 75, 38402, Saint Martin d'Hères, France

Abstract

In-situ straining experiments were performed on pure copper to investigate dislocation motion under heavy ion irradiation at high stress levels. The unpinning of dislocations from irradiation defects followed by glide was observed under irradiation at stress level just below the critical stress for dislocation glide without irradiation. This phenomenon was unraveled for the first time in copper. The dislocation dynamics recorded in-situ was statistically analyzed using digital image processing to determine the pinning lifetime. Quantitative analysis of pinning lifetimes have been performed, suggesting that a cascade related mechanism is operative to explain the fast dislocation glide under irradiation. This work provides a new insight on the irradiation creep deformation at high stress level.

Keywords: *In-situ* transmission electron microscopy (TEM), ion irradiation, copper, Irradiation creep

1. Introduction

Irradiation creep is a viscoplastic deformation mechanism occurring in components inside nuclear reactors subjected to constant load and long term irradiation. Structural materials such as austenitic steels and zirconium alloys undergo irradiation creep that must be properly characterized and predicted for safe operation. Usually, irradiation creep experiments are conducted on bulk material samples within test reactors under combined fast neutron flux and applied mechanical load [1, 2]. However, such experiments suffer from major drawbacks such as long irradiation periods, activation of the test material, and no option for *in-situ* characterization of the elementary physical mechanisms at the origin of the macroscopic behavior. Therefore, although the macroscopic phenomenology for irradiation creep is relatively well rationalized, the underlying microscopic mechanisms are still unclear. Many theoretical mechanisms have been proposed for this phenomenon, all involving atomic displacements and creation of vacancies and interstitials under fast neutron irradiation. However, these models differ on the detailed processes explaining the point defect redistribution under stress.

Yet, due to limited experimental evidence, a controversy exists for selecting the relevant controlling mechanisms [3, 4].

An alternative to in-reactor irradiation creep experiments is to couple small scale mechanical testing and ion irradiation to accelerate the experiments while taking into account the much lower penetration of ions compared to neutrons. Jung et al. [5] and Xu et al. [6] developed specific experimental apparatus to deform materials under high-energy light ion flux with specimen thickness of the order of $100\ \mu m$. However, light ions do not simulate well the neutron damage and induce the activation of the matter [7]. An alternative approach is to use heavy ions, which better simulate the neutron damage and do not activate the matter, but have an even more limited penetration than light ions. Despite the efforts of few research teams to use miniaturized specimen coupled with heavy ion beams [7, 8, 9, 10, 11, 12, 13, 14, 15], the access to the underlying irradiation creep mechanisms remains indirect. The *in-situ* imaging of crystal defects under both straining and heavy ion irradiation inside a TEM can allow for a direct access to the active mechanisms [16]. However, until recently, TEM *in-situ* straining experiments have mainly focused on post irradiation deformation, to determine for instance the nature of the interactions between dislocations and irradiation induced defects [17, 18, 19, 20, 21, 22].

A new methodology was developed by Gaumé et al. [23] for *in-situ* deformation experiments inside a TEM under krypton ion irradiation to study high stress irradiation creep on a recrystallized zirconium alloy at room temperature and at 450°C. The authors observed that, at high stresses, irradiation induces the release and glide of dislocations pinned on irradiation defects. The objective of the present work is to conduct in-situ TEM irradiation experiments on pure copper to provide quantitative data on dislocation dynamics, to determine if the conclusions of Gaumé et al. [23] also apply to copper, and to critically assess the existing models. Copper is often considered as a model material for metals with FCC crystal structure such as austenitic steels, thus motivating this choice.

2. Experimental methods

2.1. Materials

Pure polycrystalline annealed OFHC copper (99.95%) specimens were cut out from thin sheets of 25 mm x 25 mm with a thickness of 0.3 mm. The specimens were mechanically polished down to 0.13 mm, then the center of the specimen was jet electropolished to be transparent to electrons using the commercial electrolyte D2 from Struers, at a temperature of -1°C and at a voltage of 8 V.

2.2. Test methods

2.2.1. Irradiation conditions

The *in-situ* deformation experiments under irradiation were carried out using the 2 MV ARAMIS ion implanter [24, 25] at the JANNuS-Orsay/SCALP platform (IJCLab, formerly CSNSM) [26, 27], which is part of the French EMIR accelerator network. The implanter is directly connected to the Transmission Electron Microscope (TEM), thus allowing for in-situ observations under irradiation. The irradiations were performed with 2 MeV Cu^+ ions and with fluxes in the range from 1.2×10^{10} up to 1×10^{11} ions/cm²/s (i.e. 9.6×10^{-5} to 8.0×10^{-4} dpa/s), although most experiments were performed at 5×10^{10} ions/cm²/s (4.0×10^{-4} dpa/s) and at 8×10^{10} ions/cm²/s (6.4×10^{-4} dpa/s). The final fluences ranged in between 7.3×10^{12} ions/cm² (5.84×10^{-2} dpa) and 1.3×10^{14} ions/cm² (1.04 dpa).

2.2.2. *In-situ* TEM loading

The specimens were installed on a GATAN single tilt deformation holder in a 200 kV TECNAI TEM, as represented in Figure 1. The deformation of the specimen is produced by applying a controlled displacement of one of the crossheads. In total, nine deformation experiments were performed. All the experiments were carried out at room temperature. The methodology is similar to the one conducted by Gaumé et al. [23]. First, the crosshead is displaced until the first dislocation motion occurs in the area of observation. Then, by either decreasing the crosshead displacement or by waiting until the stress relaxes sufficiently, the dislocations stop or their velocity reduces significantly. In the following, the total cross-head displacement (from the beginning of the experiment) is noted δ and dδ represents the variation in crosshead displacement. The dislocation motions are recorded using a GATAN wide angle camera during successive sequences, each sequence consisting on a first step of a few tens of seconds during which the ion beam is off, followed by a second step of a few tens of seconds during which the ion beam is switched on, followed by a third step of a few tens of seconds with the ion beam turned off again. Between two sequences, the crosshead displacement can be increased and the ion flux can be modified.

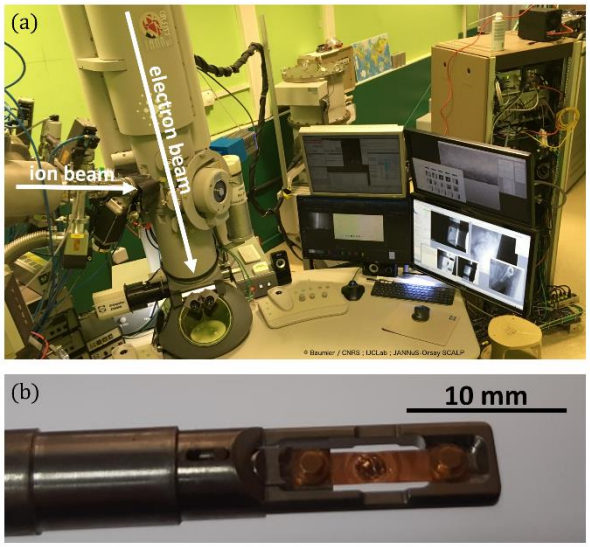

Figure 1 – (a) JANNuS-Orsay SCALP modified Tecnai G20 TEM allowing for ion beam irradiation with an angle between the electron and ion beams of 68° [27] – (b) Head of the deformation GATAN TEM single tilt sample holder.

2.3. Image analysis procedures

One of the main objectives of the experiments is to observe the dislocation motion successively during or after ion irradiation. In order to estimate the jump length or dislocation mean free path, an image analysis procedure presented in Figure 2 has been set up using the image processing program Fiji [28]. A line (in red in Figure 2) is first defined along the dislocation glide direction covering the whole distance travelled by the dislocation during the sequence of images. The kymograph of this frame sequence along this line is then computed. A kymograph [29, 30] represents the intensity of the pixels along a defined line for successive frames. Given that the dislocations have a black contrast, the kymograph gives the position of the dislocation along the glide direction as a function of the frame number. The kymograph is then segmented manually in order to only select the dislocation path, and the skeleton [31] of the image is extracted. A skeletonization consists in the reduction of binary objects into one pixel wide objects. The white curve generated is then exported, and the position and the frame are converted respectively in nanometers and seconds. Nonetheless, since the glide plane is not the image plane, it is important to note that the distances thereby obtained are projected distances. Therefore, the images are first corrected using a geometrical transformation before the image procedure presented is implemented. The details of this geometrical transformation can be found in

the Supplementary data. For instance, the results of this procedure performed on six dislocations during an irradiation step are provided in Figure 3. Another useful tool often used to analyze TEM image sequences is the image subtraction. This tool allows the determination of the variation on an image between two frames, and thus, in our case, of the dislocation displacements.

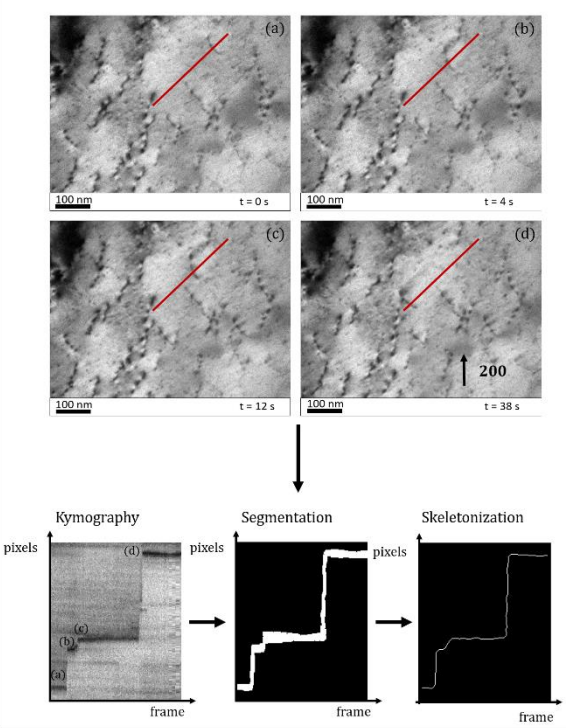

Figure 2 – Dislocation motion analysis using the image processing program Fiji [28].

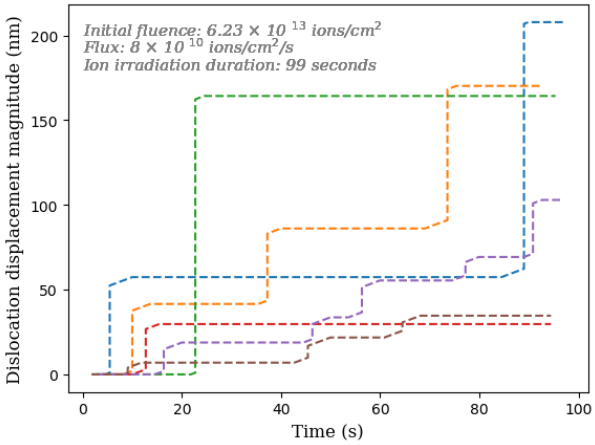

Figure 3 – Evolution of the magnitude of the displacement of several dislocations during an irradiation step.

3. Experimental results

3.1. *In-situ* straining experiments under irradiation

3.1.1. General observations

3.1.1.1. First irradiation step

Prior to any irradiation, the crosshead is displaced until the first dislocation glides are observed. The local stress is thus equal to the critical stress for dislocation motion. For instance, in Figure 4.e,f, the

dislocations glide after two successive increments in crosshead displacement. If the crosshead displacement is not increased further, the dislocations stop moving because of the stress relaxation. The local stress in thus now just below the critical stress for dislocation motion. After a few tens of seconds, the ion beam is turned on, while the crosshead displacement is held constant. During this first ion irradiation step, the dislocations remain immobile (Figure 4.d,h). After the irradiation, the crosshead displacement must be significantly increased to induce again the glide of these dislocations. The dislocations are now pinned by irradiation defects and their motion occurs by glide through these defects. This suggests that irradiation induces the unpinning of dislocations from irradiation defects. A film showing this sequence is provided as Supplementary Data (Video 1). This dislocation pinning phenomenon is consistent with previous post-irradiation straining experiments [32, 18, 33, 34]. The dislocations observed in this sequence present a V-shape and the motion of the tip of the V-shape is along the $[110]$ axis. Moreover, the extinctions of the dislocations are consistent with a $\frac{1}{2}[110]$ Burgers vector and the slip traces are consistent with the glide planes $(1\bar{1}1)$ and $(\bar{1}11)$. This indicates that a segment of each dislocation cross-slipped between two glide planes $(1\bar{1}1)$ and $(\bar{1}11)$. More details on this analysis can be found in the Supplementary Data.

3.1.1.2. Further irradiation steps

Before the subsequent irradiation step, the crosshead displacement is significantly increased to reach the new critical stress for dislocation motion. The dislocations presented in the Figure 4 start to slightly glide along short distances. If the crosshead displacement is held constant, they stop moving, because of progressive stress-relaxation. The local applied stress is now just below the new critical stress needed to make the dislocations move through irradiation defects. As earlier, after a few tens of seconds, the ion beam is turned on, with the crosshead displacement kept constant. The dislocations start to slightly glide under irradiation. When the ion beam is turned off, they stop moving. This suggests that irradiation induces the unpinning of dislocations from irradiation defects. A film showing this sequence is provided as Supplementary Data (Video 1). It is also observed that other dislocations glide much faster under irradiation. These dislocations are newly generated from cracks and grain boundaries. They are less jogged, compared to initial dislocations that have absorbed point defects under irradiation, and are therefore less pinned. As for the initial dislocations, these newly generated dislocations are also immobile when the ion beam is off and start to glide under ion irradiation (Figure 5). Furthermore, under irradiation, the motion of these dislocations is not continuous and smooth. The dislocations move through series of jumps, probably from obstacle to obstacle. When following on the frame sequence the endpoints of dislocations, straight lines can be drawn suggesting that, during jumps, the motion occurs by glide. This resembles the pinning-unpinning motion under irradiation observed by Gaumé et al [23]. Films showing this sequence along with other sequences are provided as Supplementary Data (Video 2 and 3). The irradiation induced glide described above was observed even at high fluences. The deformation experiments were performed until the contrast did not permit any clear detection of dislocation motion due to the high density of irradiation defects or until the local stress decreases due to stress redistribution within the thin foil, for instance because of crack opening.

The effect of the flux was also investigated. For a flux of 1.2×10^{10} ions/cm²/s, very little motion was observed under irradiation, in comparison with higher fluxes, suggesting that for weak fluxes, the hardening effect of irradiation prevails over the irradiation induced motion of dislocations. For fluxes of 3×10^{10}, 5×10^{10} and 8×10^{10} ions/cm²/s, no significant differences depending on the flux was observed.

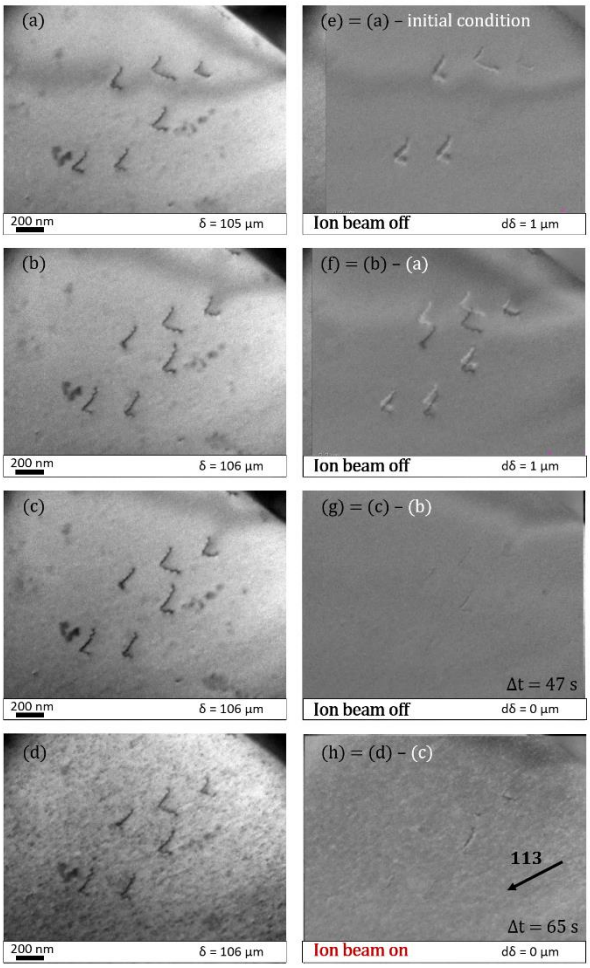

Figure 4 – TEM images showing ion beam-on and beam-off dislocation motion under applied stress: (a) and (b) two successive strain increments – (c) no strain increment – (d) a first irradiation step; (e) (f) (g) and (h): images subtractions showing in white the dislocation positions at the initial time step respectively after a first load increment, a second load increment, a waiting step of 47 seconds, and an irradiation step of 65 seconds. δ and dδ represent respectively the total cross-head displacement (since the beginning of the experiment) and the variation in crosshead displacement.

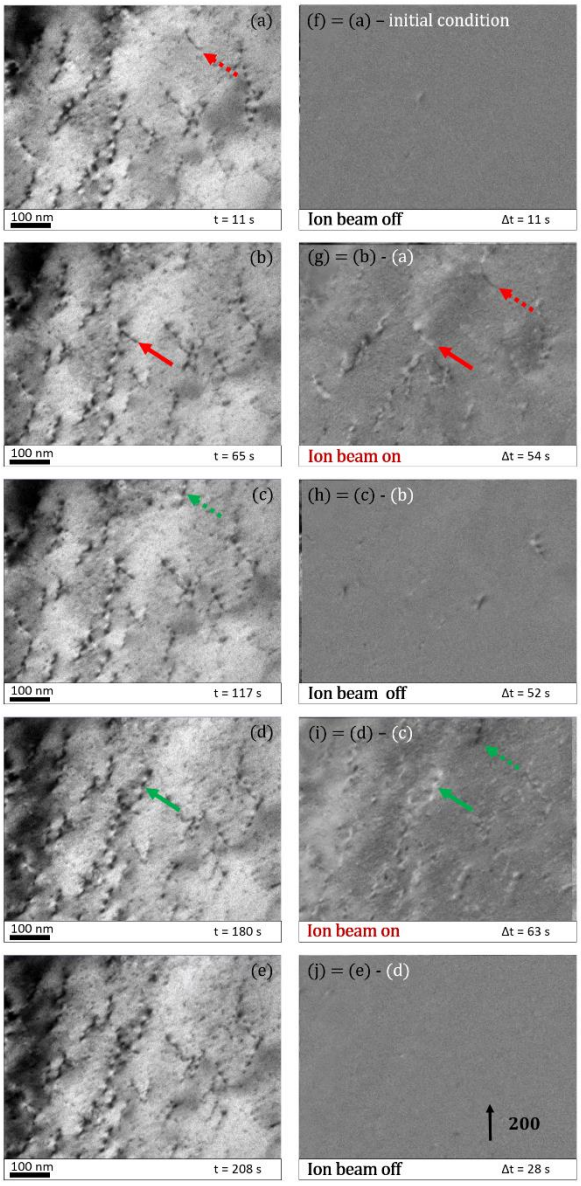

Figure 5 – TEM micrographs under applied stress (a) before irradiation, (b) at the end of a first irradiation step, (c) 50 seconds after the end of the first irradiation, (d) at the end of a second irradiation step, (e) 27 seconds after the end of the second irradiation; (f)-(j): image subtractions showing the initial dislocation positions in white. The arrow points at moving dislocations tracked during the irradiation phases. Bright Field TEM, g = 200, close to zone axis $[01\bar{2}]$*. The crosshead displacement is held constant (δ = 105 µm).*

3.1.2. Statistical study of dislocation dynamics

One experiment conducted on one area of a chosen specimen has been selected for more quantitative analysis. The crystallographic orientation of the grain is determined using electron diffraction data. The glide planes are determined based on the movements of the endpoints of the dislocations. The specimen thickness can be deduced from the orientation of the glide plane and from the projected distance between the two slip traces of the dislocation (more details can be found in the Supplementary Data). Three types of dislocations are observed in the sequence: screw dislocations gliding in the plane $(1\bar{1}\bar{1})$ with a Burgers vector $\frac{1}{2}[\bar{1}0\bar{1}]$, screw dislocations gliding in the plane $(11\bar{1})$ with a Burgers vector equal to $\frac{1}{2}[\bar{1}0\bar{1}]$, and dislocations gliding in the plane $(11\bar{1})$. The screw nature of the two first dislocation types were determined based on the cross-slip observed from the plane

$(1\bar{1}\bar{1})$ to the plane $(11\bar{1})$. The nature and Burgers vector of the last dislocation family could not be ascertained. The sample thickness in the area of observation is found to be around 80 to 100 nm. The tensile loading direction is close to the $[100]$ axis. In the following, the origin of time is taken to be the start of the experiment (from the first crosshead displacement, before any irradiation), although the sequence only concerns the irradiation steps from the 4th irradiation step (after a cumulated dose of 1.22×10^{13} ions/cm²).

3.1.2.1. Estimation of the dislocation jumps frequency

Image subtractions are performed between frames taken one second apart to measure the number of dislocation jumps per second. If a dislocation appears with a contrast on the image subtraction, it means that the dislocation has moved and this is counted as one instantaneous jump per second. If ten dislocations appear with a contrast on the image subtraction, this is counted as ten instantaneous jumps per second. This measure will be referred to, in the following, as the dislocation jump frequency. The number of dislocation jumps measured for each image subtraction can also be added up all along the experiment. This will be referred to as the cumulated number of dislocation jumps. As shown in Figure 6, the cumulated number of dislocation jumps increases sharply when the ion beam is on. The increase in dislocation motion under irradiation is relatively linear with time, and the slope, i.e. the dislocation motion frequency, is around one jump per second, compared with 0.1 jump per second when the ion beam is off.

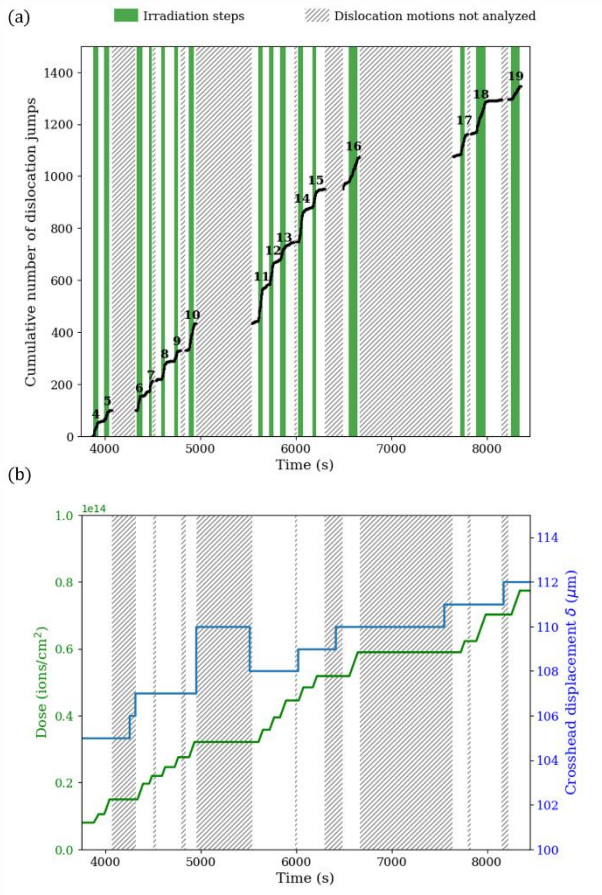

Figure 6 – Evolution with the time of (a) the cumulated number of dislocation jumps; (b) the dose and crosshead displacement δ. The origin of times is taken to be the beginning of the experiment.

3.1.2.2. Sensitivity to stress

As stated earlier, if the local stress is far below the critical stress for dislocation motion, no irradiation induced glide is observed. Just below this critical stress, dislocations start to glide under irradiation. This shows that there is a high sensitivity to the applied stress. This is further illustrated when the stress relaxes. Figure 7 represents the dislocation motion frequency over five irradiation steps. This figure shows that when there is no increase of crosshead displacement in between irradiation steps (i.e the crosshead displacement δ remains constant), the frequency of dislocation jumps under irradiation progressively drops. This is most likely due to stress relaxation. A slight increase in crosshead displacement (in between the 13th and 14th irradiation step) induces a significant increase of the jump frequency under irradiation (in green). This shows that the jump frequency under irradiation exhibits a significant sensitivity to the local stress. Consequently, the irradiation induced unpinning mechanism observed is highly sensitive to the applied stress. This figure also shows that this slight increase in crosshead displacement does not significantly affect the jump frequency when the ion beam is off (in grey). Note that the stress level is not directly measured, but the sensitivity to the crosshead displacement reflects the sensitivity to stress.

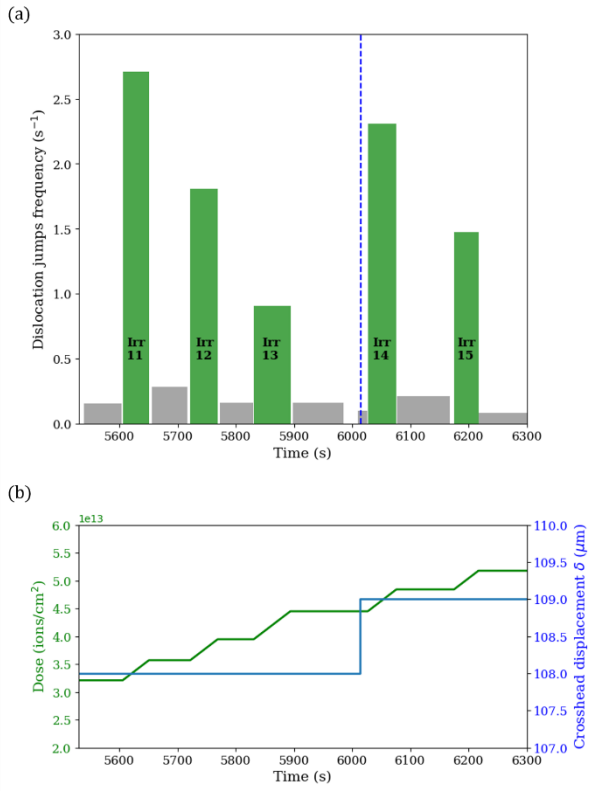

Figure 7 – (a) Dislocation jumps frequency during steps when the ion beam is off (in grey) and the ion beam is on (in green); (b) variation of the dose and crosshead displacement as a function of the time. The blue dotted line on the first graph represents the increase in crosshead displacement.

3.1.2.3. Estimation of the dislocation mean free path

Under irradiation, the dislocation motion is not smooth, but occurs by series of jumps, probably associated to the glide from obstacle to obstacle. In order to estimate the jump length or dislocation mean free path, the image analysis procedure presented in section 2.3 was used. Figure 8.a and Figure 8.b represent, respectively, the mean distances travelled during 8 irradiation steps and the histogram of the jump distances (i.e. distance travelled by a dislocation during a jump). The travelled distances remain approximatively the same for the different steps (with a slight decrease with increasing step

number). The majority of displacements are under 50 nm and the mean displacement magnitude is of 45 nm. In between two jumps, the dislocation stops moving, as seen in Figure 3, probably pinned on defects, and this waiting time is analyzed. Figure 8.c and Figure 8.d represent respectively the mean pinning lifetimes (or waiting time between two jumps) during eight irradiation steps and the histogram of mean pinning lifetimes. The mean pinning lifetime slightly increases with the irradiation dose, suggesting that the pinning ability, or obstacle strength, of irradiation defects increases with irradiation dose. The mean pinning lifetime is equal to 42 seconds.

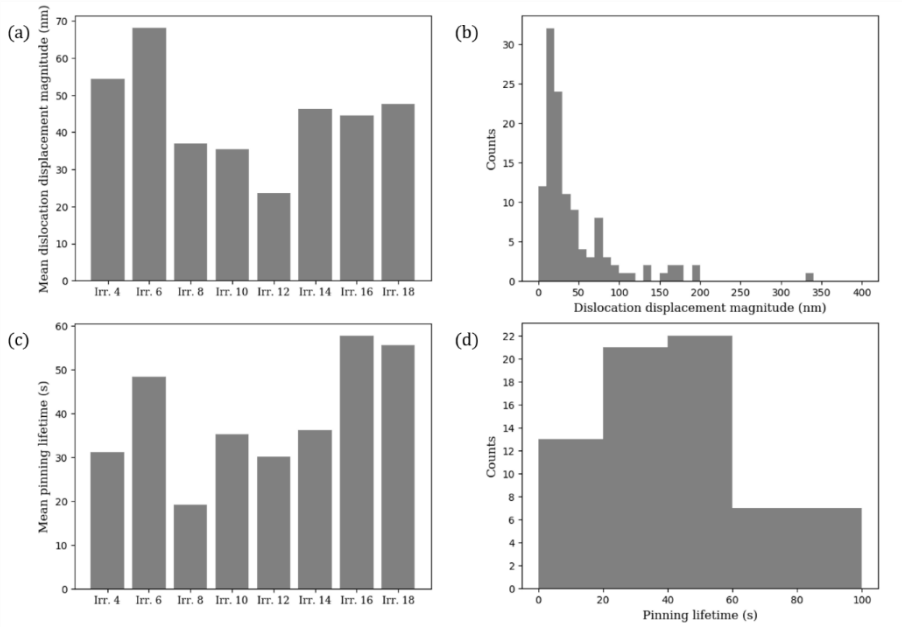

Figure 8 – (a) Mean dislocation displacement magnitude and (c) mean pinning lifetime during different irradiation steps. Distribution of (b) dislocation displacement magnitudes and (d) pinning lifetimes during irradiation from the 4th to the 18th irradiation step.

3.2. Post irradiation microstructural examination

Post-mortem analyses were performed on the sample studied in section 3.1.2 in order to characterize the irradiation defects. A weak beam image of the sample is presented in Figure 9. A high density of very small defects with a diameter of less than 3 nm is observed. The defects appear to be mainly small loops, although few SFT are also observed. However, considering the high density and small size of the defects as well as the possible overlap between these defects, the loop and SFT populations can be confused. The mean defect diameter d is estimated to be around 2 nm. Given that the mean defect density N is found around 10^{23} m^{-3}, the average defect planar spacing l can then be evaluated using:

$$l = \frac{1}{\sqrt{Nd}}. \quad (2)$$

The average defect planar spacing is around 70 nm, which is in the same order of magnitude as the dislocation mean free path (45 nm) previously estimated.

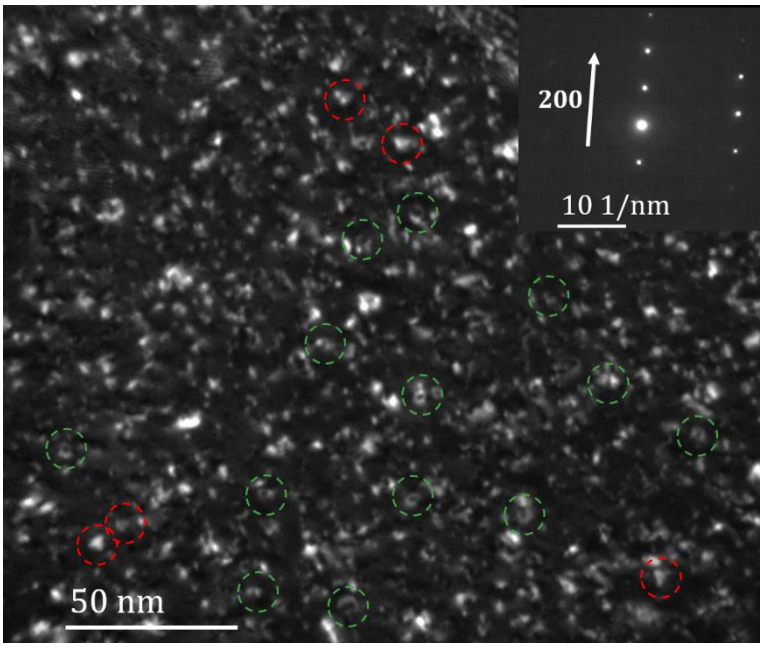

Figure 9 – TEM micrograph of the sample at the end of the experiment observed in weak beam dark field conditions with a g=200. The green and red dashed circles overlay respectively small loops and small SFT.

4. Discussion

4.1. Estimation of the mean pinning lifetime

In the sequence described above (section 3.1.2), the dislocation mean free path is equal to 45 nm, and the estimated average loop spacing in the glide plane is equal to 70 nm. Moreover, the dislocation lengths are estimated to be in the range 80 to 150 nm, with a mean dislocation length of around 100 nm (after a projection of the image on the appropriate glide plane). One can thus assume that there is, on average, one obstacle per dislocation. Therefore, the fact that the dislocation mean free path corresponds to the average distance between obstacles in the glide plane suggests that the "stop and go" motion observed is due to a pinning-unpinning of dislocations from irradiation-induced defects.

As a first approximation, we consider here that every recorded dislocation jump results from the unpinning of one dislocation from one irradiation defect. The total dislocation length observed in the sequence is equal to 2 µm. Taking a mean separation distance between pinning points of 50 nm, there are thus 40 pinning points in total in the sequence. We have recorded on average 0.1 dislocation jumps per second when the ion beam is off and 1 jump per second when the ion beam is on. This suggests a mean pinning lifetime of 40 seconds under irradiation and 400 seconds without irradiation (thermally activated glide). The mean pinning lifetime calculated using these average values is very close to the mean measured dislocation pinning lifetime of 42 seconds measured using the detailed histograms (Figure 8.d). This, again, supports the mechanism proposed which consists of the pinning-unpinning of dislocations from obstacles.

4.2. Possible irradiation creep mechanisms

In order to ensure that the unpinning event is indeed triggered by irradiation and does not result from ion beam heating effects, an estimation of the specimen heating during ion irradiation is computed and detailed in Supplementary Data. The ion irradiation induced increase in temperature appears to be low (less than 1 K). Moreover, the surface power lost in the specimen during ion irradiation is orders of magnitude lower than the surface power lost by the electron beam, which does not contribute to significant heating in conductive metals. Additional experiments, reported in Supplementary data,

have been conducted to investigate the respective contributions of electron and ion beam heating. These calculations and experiments confirm that the phenomenon under investigation here is due to irradiation effects and does not result from ion beam heating effects.

Irradiation has two distinct effects. First, it induces the generation of defects such as SFT and loops that act as obstacles to dislocation motion causing a retarded creep. The second effect enhances creep; this is the irradiation creep. In our experiments, both effects are observed: an irradiation induced hardening and a glide based irradiation creep mechanism. The glide mechanisms can either be climb assisted glide resulting from homogeneous generation and diffusion of point defects [35, 36, 37], or direct cascade induced unpinning of dislocations. This last mechanism can result from dissolution of pinning points by interaction with the cascade or by the local production of point defect due to the cascade leading to dislocation climb over the obstacle [38, 4].

There are three usual climb-assisted glide mechanisms. The first one is the dislocation bias driven climb mechanism, which results from a stronger elastic interaction between edge dislocations and interstitials than between edge dislocations and vacancies. There are two other mechanisms referred to as stress-induced preferential absorption of point defects (SIPA) mechanisms. The first one is the SIPA-I (for Stress Induced Preferential absorption due to Inhomogeneity effects) which results from polarizability effects [35, 39]. The second one is the SIPA-AD (for Stress Induced Preferential absorption due to Anisotropic Diffusion) which is due to elasto-diffusion and is considered to be a first order effect [36].

Our experimental results are compared with standard irradiation creep models proposed in the literature. All the quantitative models are based on rate theory. Several strong hypothesis are made for these models [4, 35, 36, 37]. The obstacles are assumed to be unshearable, although the reality is more complex since dislocation-loop reactions are known to occur [40, 41, 42, 17]. The production of point defects is considered spatially and temporally homogeneous, which is a quite simple assumption since the point defects are produced by stochastically generated displacement cascades. The climb duration, calculated using this model, that should correspond to the mean pinning lifetime, is found to be at least 30 times longer than in the experiments and does not show the same sensitivity to stress. More details about this analysis can be found in the Supplementary Data. Therefore, either the hypothesis of the model chosen are too simple, or another mechanism, resulting from cascade effects, may be operative. For instance, a displacement cascade induced climb mechanism can be considered [38]. However, the climb based mechanisms only concern edge dislocations, and do not apply to the screw dislocations observed in our experiments. Very recently, Khiara et al. [43] showed through molecular dynamics simulations performed on pure zirconium and for stresses just below the yield stress, the release of screw dislocations pinned on small loops by displacement cascades generated by irradiation. After the unpinning of the dislocation, it was observed that the freed dislocation is now straight and that the loop is partially destructed. For stresses just below the critical stress for dislocation unpinning, the pinning lifetimes estimated based on molecular dynamics calculations are in the same range as the experimental lifetimes. This new mechanism, if extended to copper, can provide an explanation to the unpinning of screw dislocations observed during our experiment.

5. Conclusion

In-situ straining experiments were performed under heavy ion irradiation on pure copper under high stress levels. The release, assisted by irradiation, of dislocations pinned on small loops has been revealed under high applied stresses, resembling the phenomenon observed by Gaumé et al. [23] for a zirconium alloy. This phenomenon, observed for the first time for pure copper, provides a new insight

on the irradiation creep deformation mechanism at high stresses. The main findings of this work are the following:

- The dislocations glide under ion beam irradiation by series of jumps, indicating the release from one pinning point, glide to the next one before being pinned again. This is supported by the fact that the dislocation mean free path, around 45 nm, is of the same order as the distance between irradiation defects.
- The underlying irradiation creep mechanism (with the ion beam switched on) is very sensitive to stress, and occurs for stresses just below the critical stress for dislocation motion (with the ion beam switched off).
- The magnitude of the flux affects the dislocation activity, since for a flux of 1.2×10^{10} ions/cm²/s very few motions were observed in comparison to higher fluxes (above 3×10^{10} ions/cm²/s)
- The mean pinning lifetime of dislocations was estimated to be around 40 seconds.
- Beam heating effects on the phenomena have been discarded.
- The traditional irradiation creep mechanisms and models that can explain the observations are the climb followed glide mechanisms, due either to dislocation bias, SIPA-I or SIPA-AD. The pinning lifetime estimated using the rate theory in the conditions of the experiments for these three mechanisms underestimate the experimental value by a factor of at least 30. Moreover, for the models for which the pinning lifetimes are the lowest, these pinning lifetimes do not show the same sensitivity to stress as in the experiments. This discrepancy between theory and experiment suggests that another mechanism, presumably cascade related, is operative to explain the much faster creep rates.

6. Acknowledgments

These experiments were supported by the French EMIR&A accelerators network. The authors are grateful to the JANNuS-Orsay/SCALP technical staff at IJCLab (formerly CSNSM) for ARAMIS ion irradiations, and technical help at the TEM during *in*-situ experiments, especially Cédric Baumier, Jérôme Bourçois, Sandrine Picard, and Cyril Bachelet.

References

[1] E. S. Aitkhozhin and E. V. Chumakov, "Radiation-induced creep of copper, aluminium and their alloys," *Journal of nuclear materials,* vol. 233, pp. 537-541, 1996.

[2] J. Garnier, Y. Bréchet, M. Delnondedieu, C. Pokor, P. Dubuisson, A. Renault, X. Averty and J. P. Massoud, "Irradiation creep of SA 304L and CW 316 stainless steels: Mechanical behaviour and microstructural aspects. Part I: Experimental results," *Journal of nuclear materials,* vol. 413, no. 2, pp. 63-69, 2011.

[3] F. A. Garner and D. S. Gelles, "Irradiation creep mechanisms: an experimental perspective," *Journal of Nuclear Materials,* vol. 159, no. 286-309, 1988.

[4] J. R. Matthews and M. W. Finnis, "Irradiation creep models—An overview," *Journal of Nuclear Materials,* vol. 159, pp. 257-285, 1988.

[5] P. Jung, A. Schwarz and H. K. Sahu, "An apparatus for applying tensile, compressive and cyclic stresses on foil specimens during light ion irradiation.," *Nuclear Instruments and Methods in Physics Research Section A: Accelerators, Spectrometers, Detectors and Associated Equipment,* vol. 234, no. 2, pp. 331-334, 1985.

[6] C. Xu and G. S. Was, " In situ proton irradiation creep of ferritic–martensitic steel T91.," *Journal of nuclear materials,* vol. 441, no. 1-3, pp. 681-687, 2013.

[7] K. Tai, R. S. Averback, P. Bellon and Y. Ashkenazy, "Irradiation-induced creep in nanostructured Cu alloys.," *Scripta Materialia,* vol. 65, no. 2, pp. 163-166, 2011.

[8] K. Tai, R. S. Averback, P. Bellon, Y. Ashkenazy and B. Stumphy, "Temperature dependence of irradiation-induced creep in dilute nanostructured Cu–W alloys.," *Journal of nuclear materials,* vol. 422, no. 1-3, pp. 8-13, 2012.

[9] S. Özerinç, R. S. Averback and W. P. King, "In situ creep measurements on micropillar samples during heavy ion irradiation.," *Journal of Nuclear Materials,* vol. 451, no. 1-3, pp. 104-110, 2014.

[10] S. Özerinç, H. J. Kim, R. S. Averback and W. P. King, "Direct measurements of irradiation-induced creep in micropillars of amorphous Cu56Ti38Ag6, Zr52Ni48, Si, and SiO2.," *Journal of Applied Physics,* vol. 117, no. 2, p. 024310, 2015.

[11] P. Lapouge, F. Onimus, M. Coulombier, J.-P. Raskin, T. Pardoen and Y. Bréchet, "Creep behavior of submicron copper films under irradiation," *Acta Materialia,* vol. 131, pp. 77-87, 2017.

[12] P. Lapouge, F. Onimus, R. Vayrette, J.-P. Raskin and T. Pardoen, "A novel on chip test method to characterize the creep behavior of metallic layers under heavy ion irradiation," *Journal of Nuclear Materials Volume 476,* vol. 476, pp. 20-29, 2016.

[13] G. S. Jawaharram, P. M. Price, C. M. Barr, K. Hattar, R. S. Averback and S. J. Dillon, "High temperature irradiation induced creep in Ag nanopillars measured via in situ transmission electron microscopy.," *Scripta Materialia,* vol. 148, pp. 1-4, 2018.

[14] G. S. Jawaharram, C. M. Barr, A. M. Monterrosa, K. Hattar, R. S. Averback and S. J. Dillon, "Irradiation induced creep in nanocrystalline high entropy alloys.," *Acta Materialia,* vol. 182, pp. 68-76, 2020.

[15] S. J. Dillon, D. C. Bufford, G. S. Jawaharram, X. Liu, C. Lear, K. Hattar and R. S. Averback, "Irradiation-induced creep in metallic nanolaminates characterized by In situ TEM pillar nanocompression.," *Journal of Nuclear Materials,* vol. 490, pp. 59-65, 2017.

[16] M. Legros, "In situ mechanical TEM: Seeing and measuring under stress with electrons.," *Comptes Rendus Physique,* vol. 15, no. 2-3, pp. 224-240, 2014.

[17] J. S. Robach, I. M. Robertson, B. D. Wirth and A. Arsenlis, "In-situ transmission electron microscopy observations and molecular dynamics simulations of dislocation-defect interactions in ion-irradiated copper," *Philosophical Magazine,* vol. 83, no. 8, pp. 955-967, 2003.

[18] J. S. Robach, I. M. Robertson, H. J. Lee and B. D. Wirth, "Dynamic observations and atomistic simulations of dislocation–defect interactions in rapidly quenched copper and gold," *Acta materialia,* vol. 54, no. 6, pp. 1679-1690, 2006.

[19] S. J. Zinkle and Y. Matsukawa, "Observation and analysis of defect cluster production and interactions with dislocations," *Journal of nuclear materials,* vol. 329, pp. 88-96, 2004.

[20] R. Schäublin, Z. Yao, P. Spätig and M. Victoria, "Dislocation defect interaction in irradiated Cu," *Materials Science and Engineering: A,* vol. 400, pp. 251-255, 2005.

[21] Y. Matsukawa and S. J. Zinkle, "Dynamic observation of the collapse process of a stacking fault tetrahedron by moving dislocations," *Journal of Nuclear Materials,* vol. 329, pp. 919-923, 2004.

[22] D. Kiener, P. Hosemann, S. A. Maloy and A. M. Minor, "In situ nanocompression testing of irradiated copper," *Nature materials,* vol. 10, no. 8, pp. 608-613, 2011.

[23] M. Gaumé, P. Baldo, F. Mompiou and F. Onimus, "In-situ observation of an irradiation creep deformation mechanism in zirconium alloys," *Scripta Materialia,* vol. 154, pp. 87-91, 2018.

[24] E. Cottereau, J. Camplan, J. Chaumont and R. Meunier, "Aramis: an accelerator for research on astrophysics, microanalysis and implantation in solids," *Materials Science and Engineering: B,* vol. 2, no. 1-3, pp. 217-221, 1989.

[25] N. Chauvin, S. Henry, H. Flocard, F. Fortuna, O. Kaitasov, P. Pariset, S. Pellegrino, M. Ruault, Y. Serruys and P. Trocelier, "Optics calculations and beam line design for the JANNuS facility in Orsay," *Nuclear Instruments and Methods in Physics Research Section B: Beam Interactions with Materials and Atoms,* vol. 261, no. 1-2, p. 2007, 34-39.

[26] Y. Serruys, P. Trocellier, S. Miro, E. Bordas, M. Ruault, O. Kaïtasov, S. Henry, O. Leseigneur, T. Bonnaillie, S. Pellegrino and S. Vaubaillon, "JANNUS: A multi-irradiation platform for experimental validation at the scale of the atomistic modelling," *Journal of Nuclear Materials,* vol. 386, pp. 967-970, 2009.

[27] C. O. Bacri, C. Bachelet, C. Baumier, J. Bourçois, L. Delbecq, D. Ledu, N. Pauwels, S. Picard, S. Renouf and C. Tanguy, "SCALP, a platform dedicated to material modifications and characterization under ion beam.," *Nuclear Instruments and Methods in Physics Research Section B: Beam Interactions with Materials and Atoms,* vol. 406, pp. 48-52, 2017.

[28] J. Schindelin, I. Arganda-Carreras, E. Frise, V. Kaynig, M. Longair, T. Pietzsch, S. Preibisch, C. Rueden, S. Saalfeld, B. Schmid and J. Tinevez, "Fiji: an open-source platform for biological-image analysis," *Nature methods,* vol. 9, no. 7, pp. 676-682, 2012.

[29] P. Dhonukshe, N. Vischer and T. W. Gadella, "Contribution of microtubule growth polarity and flux to spindle assembly and functioning in plant cells," *Journal of Cell Science,* vol. 119, no. 15, pp. 3193-320, 2006.

[30] H. M. Zhou, I. Brust-Mascher and J. M. Scholey, "Direct visualization of the movement of the monomeric axonal transport motor unc-104 along neuronal processes in livingcaenorhabditis elegans," *Journal of Neuroscience,* vol. 21, no. 11, pp. 3749-3755, 2001.

[31] I. Arganda-Carreras, R. Fernández-González, A. Muñoz-Barrutia and C. Ortiz-De-Solorzano, "3D reconstruction of histological sections: Application to mammary gland tissue," *Microscopy research and technique,* vol. 73, no. 11, pp. 1019-1029, 2010.

[32] M. Briceño, J. Fenske, M. Dadfarnia, P. Sofronis and I. M. Robertson, "Effect of ion irradiation-produced defects on the mobility of dislocations in 304 stainless steel," *Journal of Nuclear Materials,* vol. 109, no. 1, pp. 18-26, 2011.

[33] F. Long, M. Daymond and Z. Yao, "Deformation mechanism study of a hot rolled Zr-2.5 Nb alloy by transmission electron microscopy. I. Dislocation microstructures in as-received state and at different plastic strains.," *Journal of Applied Physics,* vol. 117, no. 9, p. 094307, 2015.

[34] D. Kaoumi and V. Jammot, "Insights into the plastic behavior of irradiated Ni-based alloy through in-situ TEM experiments: Formation and evolution of defect-free channels.," *Journal of Nuclear Materials,* vol. 523, pp. 33-42, 2019.

[35] C. H. Woo, "Effects of an anisotropic dislocation structure on irradiation creep due to stress induced preferred absorption of point defects," *Journal of Nuclear Materials,* vol. 80, no. 1, pp. 132-143, 1979.

[36] C. H. Woo, "Irradiation creep due to elastodiffusion," *Journal of Nuclear Materials,* vol. 120, no. 1, pp. 55-64, 1984.

[37] R. Bullough, M. R. Hayns and M. H. Wood, "Sink strengths for thin film surfaces and grain boundaries," *Journal of Nuclear Materials,* vol. 90, no. 1-3, pp. 44-59, 1980.

[38] R. E. Voskoboinikov, "nteraction of collision cascades with an isolated edge dislocation in aluminium.," *Nuclear Instruments and Methods in Physics Research Section B: Beam Interactions with Materials and Atoms,* vol. 303, pp. 125-128, 2013.

[39] R. Bullough and J. R. Willis, "The stress-induced point defect-dislocation interaction and its relevance to irradiation creep," *Philosophical Magazine,* vol. 31, no. 4, pp. 855-861, 1975.

[40] D. Terentyev, P. Grammatikopoulos, D. J. Bacon and Y. Osetsky, "Simulation of the interaction between an edge dislocation and a< 1 0 0> interstitial dislocation loop in α-iron.," *Acta Materialia,* vol. 56, no. 18, pp. 5034-5046, 2008.

[41] E. Rodary, D. Rodney, L. Proville, Y. Bréchet and G. Martin, "Dislocation glide in model Ni (Al) solid solutions by molecular dynamics.," *Physical Review B,* vol. 70, no. 5, p. 054111, 2004.

[42] D. Rodney, "Molecular dynamics simulation of screw dislocations interacting with interstitial frank loops in a model FCC crystal.," *Acta Materialia,* vol. 52, no. 3, p. Acta Materialia, 2004.

[43] N. Khiara, F. Onimus, L. Dupuy, W. Kassem, J. Crocombette, T. Pardoen, J. Raskin and Y. Bréchet, "A novel displacement cascade driven irradiation creep mechanism in α-zirconium: A molecular dynamics study.," *Journal of Nuclear Materials,* p. 152336, 2020.